Supplementary Material

Cellular thermometry considerations for probing biochemical pathways

Manjunath C. Rajagopal[1], and Sanjiv Sinha[1*].

[1]*Department of Mechanical Science and Engineering, University of Illinois at Urbana-Champaign, Urbana, IL 61801, USA.*

Section 1: Finite element analysis description

Throughout this work, we use finite element analysis using COMSOL Multiphysics. We first validate the finite element analysis for a generalized scenario involving transient heat release from a cell placed in an infinite medium.

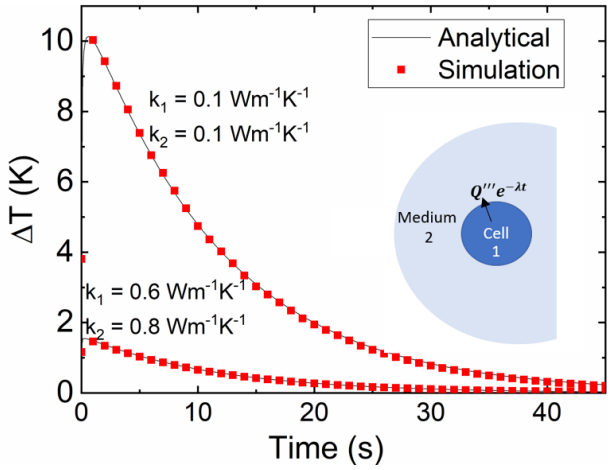

Figure S1. Validating the finite element model for a generalized transient heat. The transient temperature change (ΔT) at the center of the cell is plotted. The temperature changes for two different combinations of cell (k_1) and medium (k_2) thermal conductivity are shown. The inset schematically depicts the domain of analysis, which is a cell of radius a, dissipating heat in an infinite medium.

Consider a transient heat $Q'''e^{-\lambda t}$ (W/m^3) diffusing from a cell (represented by 1) of radius a, in an infinite medium (represented by 2), shown schematically in Figure S1. The heat diffusion equation in spherical coordinates at a radius $r < a$ is given by:

$$\frac{1}{r^2}\frac{\partial}{\partial r}\left(r^2 k_1 \frac{\partial T}{\partial r}\right) + \ Q'''e^{-\lambda t} = \rho_1 C_1 \frac{\partial T}{\partial t} \tag{1}$$

where, T is the temperature, ρ_1 is the cell's density, C_1 is the cell's specific heat capacity, t is the time and r is the distance from the center of the cell. At a radius $r > a$, the heat diffusion equation is:

$$\frac{1}{r^2}\frac{\partial}{\partial r}\left(r^2 k_2 \frac{\partial T}{\partial r}\right) = \rho_2 C_2 \frac{\partial T}{\partial t} \tag{2}$$

where, ρ_2 is the medium's density, C_2 is the specific heat capacity of the surrounding medium. The temperature boundary condition at a radius $r = a$, is given by,

$$k_1 \left|\frac{\partial T}{\partial r}\right|_{r=a^-} = k_2 \left|\frac{\partial T}{\partial r}\right|_{r=a^+} \tag{3}$$

We use the Laplace transformation technique described in a similar previous work [1] to solve equations (1)-(3) to obtain the temperature distribution inside the cell ($r < a$) as:

$$T(r,t) = \frac{a^2 Q'''}{k_1}\left\{\left(\frac{1}{3}\frac{k_1}{k_2} + \frac{1}{6} - \frac{r^2}{6a^2}\right)e^{-\lambda t} - \frac{2ab}{r\pi}\int_0^\infty \frac{e^{-\frac{y^2 t}{\gamma_1}}}{(y^2 - \lambda\gamma_1)}\frac{(\sin y \ - y\cos y)\sin\frac{ry}{a}\, dy}{[\,(c\sin y \ - y\cos y)^2 + b^2 y^2 \sin^2 y]}\right\} \tag{4}$$

Where, a is the radius of the cell, $b = \frac{k_2}{k_1}\sqrt{\frac{\alpha_1}{\alpha_2}}$, α is the thermal diffusivity, $c = 1 - k_2/k_1$.

We compare the results of the analytical model with that of a 3D finite element model in Figure 1. The specific heat capacity for the cell and medium were taken to be 2900 J.kg^{-1}K^{-1} and 4100 J.kg^{-1}K^{-1}, respectively [2], [3]. The density of the cell and medium is 1000 kg.m^{-3} and 1010 kg.m^{-3}, respectively. We considered a cell of radius 30 μm dissipating 300 $e^{-t/10}$ μW of heat. For different combinations of k_1 and k_2, we shown in Figure 1 that the finite element model matches the analytically predicted temperature change at the center of the cell. This validated finite element model is representative of all the simulations reported in this work. We also performed mesh convergence tests to identify the required mesh density such that all the results shown in the manuscript are independent of the mesh.

Section 2: Effective thermal conductivity approximation analysis

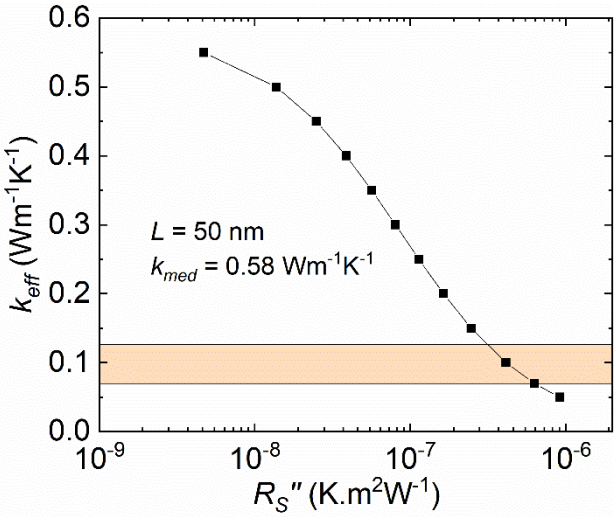

Figure S2. A high resistance R_S'' reduces the effective thermal conductivity k_{eff}. The R_S'' shown here corresponds to a length-scale L=50 nm and k_{med}=0.58 Wm^{-1}K^{-1}. The shaded region corresponds to a k_{eff}: 0.07 – 0.13 Wm^{-1}K^{-1}, which was recently reported [4] to be the range of effective thermal conductivity at intracellular regions.

Section 3: Bio-heat transport model

The bio-heat transport model is useful to study heat transport in tissues that are far from large blood vessels. In such tissues, the blood flow is assumed to result in uniform volumetric heat production, $Q_b''' = \rho_b \omega_b C_b (T_b - T)$, where ρ_b is the density, C_b is the specific heat of the blood, T_b= 37.1°C is the arterial blood temperature, T is the local tissue temperature, and ω_b is the blood perfusion rate at the tissue [5], [6]. Physiologically, the blood perfusion sustains the nutrient supply to the tissue to maintain a metabolic heat, Q_{met}''' at the tissue, and also functions to stabilize the temperature (thermoregulation) in the tissue. We model the BAT deposit near the skin of the supraclavicular region. The physical and thermal properties of the tissues are summarized in Table S1. We used the following blood properties: density (1043 kg.m^{-3}), and specific heat (3825 J.kg^{-1}K^{-1}) [7].

Table S1: List of thermal and physical properties of the tissues. Refer [6], [8] for more details.

Tissue	**Density (kg.m^{-3})**	**Specific heat (J.kg^{-1}K^{-1})**	**Thermal conductivity (Wm^{-1}K^{-1})**	**Metabolic heat, Q_{met}''' (W.m^{-3})**	**Blood perfusion rate, ω_b (s^{-1})**	**Dimensions**
Skin	1109	3391	0.37	1827	1.97×10^{-3}	1.5 mm (*t*)
WAT	911	2127	0.18	462	4.98×10^{-4}	10 mm (*t*)
BAT	911	2503	0.26	2579	1.17×10^{-3}	2 cm (*a*), 1 cm (*b*)
Muscle	1090	3421	0.49	1052	7.15×10^{-4}	200 mm (*t*)

Figure S3a shows the computational model representative of the supraclavicular region BAT deposits. BAT volumes vary depending on the age, location, and weight of the individual. Here, we use a 2 cm^3 BAT as an example to identify the typical temperature changes expected in tissues of length-scale ~20 mm [6], [9], [10]. Under cold stimulation ($T_{ambient}$=15°C), the BAT metabolism can be expected to increase by up to 25-fold in humans [11], [12]. In Figure S3b, we show the temperature contour for a 25-fold increase in BAT metabolism. Figure 8b in the manuscript shows the temperature change for 5, 10, 15, 20, 25-fold increase in BAT metabolism. The blood perfusion rate (ω_b) is also correspondingly increased, since it is the source of nutrients to sustain the metabolism. Further, we assume that the blood perfusion is reduced by 60% due to cold exposure [13]. A convective heat transfer boundary condition (h=5 Wm^{-2}K^{-1}) is used at the skin. The remaining boundaries are treated as adiabatic. Additional details on this bio-heat transport model can be found in other studies [5], [6].

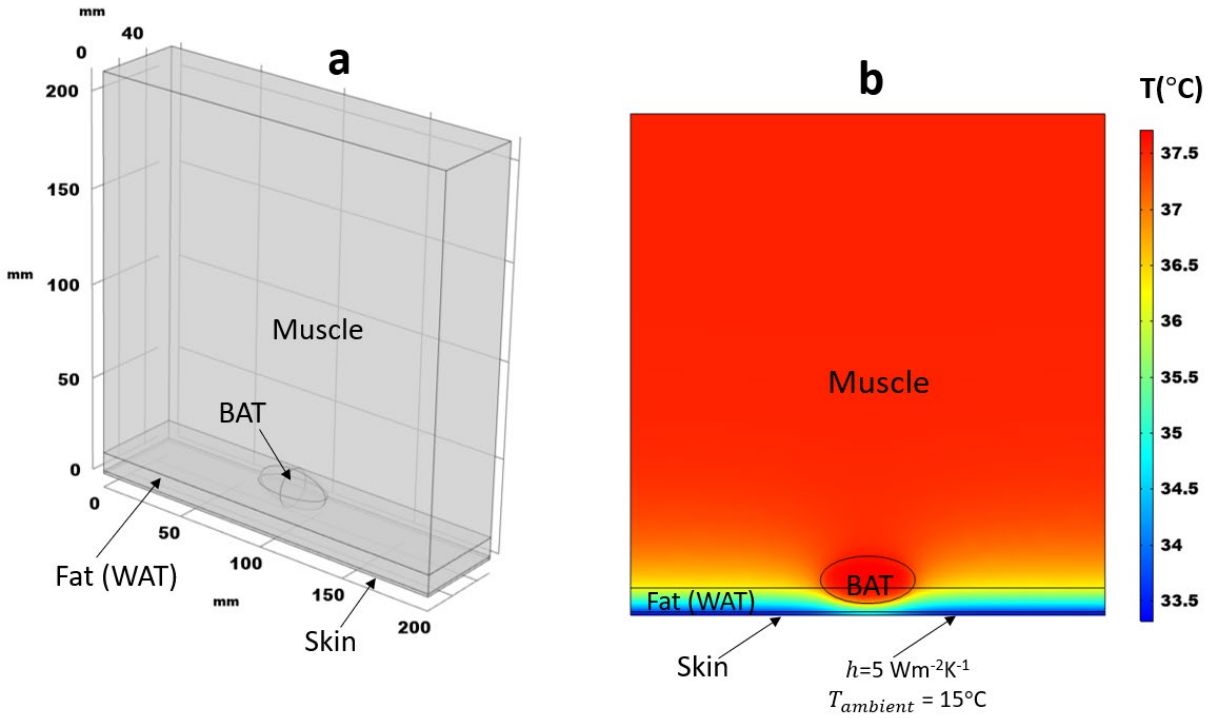

Figure S3. a) A schematic of the computational domain used for the bio-heat transport model of the supraclavicular region. The dimensions and physical properties are given in Table 1. b) A cross-sectional temperature contour of the tissues under cold stimulation with a 25-fold increase in BAT metabolism.

Supplementary References:

[1] T. A. Balasubramaniam and H. F. Bowman, "Temperature Field Due to a Time Dependent Heat Source of Spherical Geometry in an Infinite Medium," *J. Heat Transfer*, vol. 96, no. 3, pp. 296–299, Aug. 1974, doi: 10.1115/1.3450195.

[2] R. T. ElAfandy *et al.*, "Nanomembrane-Based, Thermal-Transport Biosensor for Living Cells," *Small*, vol. 13, no. 7, Art. no. 7, 2017, doi: 10.1002/smll.201603080.

[3] M. H. Sharqawy, J. H. L. V, and S. M. Zubair, "Thermophysical properties of seawater: a review of existing correlations and data," *Desalination and Water Treatment*, vol. 16, no. 1–3, pp. 354–380, Apr. 2010, doi: 10.5004/dwt.2010.1079.

[4] S. Sotoma *et al.*, "In situ measurement of intracellular thermal conductivity using heater-thermometer hybrid diamond nanosensor," *bioRxiv*, p. 2020.06.03.126789, Jun. 2020, doi: 10.1101/2020.06.03.126789.

[5] J. Crezee and J. J. W. Lagendijk, "Experimental verification of bioheat transfer theories: measurement of temperature profiles around large artificial vessels in perfused tissue," *Phys. Med. Biol.*, vol. 35, no. 7, pp. 905–923, Jul. 1990, doi: 10.1088/0031-9155/35/7/007.

[6] D. B. Rodrigues *et al.*, "Numerical 3D modeling of heat transfer in human tissues for microwave radiometry monitoring of brown fat metabolism," *Proc SPIE*, vol. 8584, Feb. 2013, doi: 10.1117/12.2004931.

[7] K. Arunachalam, P. F. Maccarini, O. I. Craciunescu, J. L. Schlorff, and P. R. Stauffer, "Thermal characteristics of thermobrachytherapy surface applicators for treating chest wall recurrence," *Phys. Med. Biol.*, vol. 55, no. 7, pp. 1949–1969, Mar. 2010, doi: 10.1088/0031-9155/55/7/011.

[8] R. P. Chhabra, *CRC Handbook of Thermal Engineering*. CRC Press, 2017.

[9] P. Lee, K. K. Y. Ho, P. Lee, J. R. Greenfield, K. K. Y. Ho, and J. R. Greenfield, “Hot fat in a cool man: infrared thermography and brown adipose tissue,” *Diabetes, Obesity and Metabolism*, vol. 13, no. 1, pp. 92–93, Jan. 2011, doi: 10.1111/j.1463-1326.2010.01318.x.
[10] W. D. van Marken Lichtenbelt *et al.*, “Cold-Activated Brown Adipose Tissue in Healthy Men,” *New England Journal of Medicine*, vol. 360, no. 15, pp. 1500–1508, Apr. 2009, doi: 10.1056/NEJMoa0808718.
[11] K. A. Virtanen *et al.*, “Functional Brown Adipose Tissue in Healthy Adults,” *http://dx.doi.org/10.1056/NEJMoa0808949*, Dec. 2009, doi: 10.1056/NEJMoa0808949.
[12] A. M. Cypess *et al.*, “Identification and Importance of Brown Adipose Tissue in Adult Humans,” *http://dx.doi.org/10.1056/NEJMoa0810780*, Dec. 2009, doi: 10.1056/NEJMoa0810780.
[13] V. Vuksanović, L. W. Sheppard, and A. Stefanovska, “Nonlinear Relationship between Level of Blood Flow and Skin Temperature for Different Dynamics of Temperature Change,” *Biophysical Journal*, vol. 94, no. 10, pp. L78–L80, May 2008, doi: 10.1529/biophysj.107.127860.